Journal of Solid Mechanics Vol. 11, No. 1 (2019) pp. 144-154
DOI: 10.22034/JSM.2019.664225

Free Vibration Analysis of Functionally Graded Piezoelectric Material Beam by a Modified Mesh Free Method

M. Froutan *, Sh. Sharafi, S. Mohammadi

Department of Mechanical Engineering, Razi University, Kermanshah, Iran

Received 9 November 2018; accepted 7 January 2019

ABSTRACT

A mesh-free method based on moving least squares approximation (MLS) and weak form of governing equations including two dimensional equations of motion and Maxwell's equation is used to analyze the free vibration of functionally graded piezoelectric material (FGPM) beams. Material properties in beam are determined using a power law distribution. Essential boundary conditions are imposed by the transformation method. The mesh-free method is verified by comparison with a finite element method (FEM) which performed for FGPM beams. Comparisons showed that this model has a good accuracy. After validation of the presented model, a parametric study was carried out to investigate the effect of mechanical and electrical boundary conditions, slenderness ratio and distribution of constituent materials on natural frequencies of FGPM beams. It is concluded that slenderness ratio has more significant effect on lower frequencies. On the other hand, higher frequencies are affected by the volume fraction power index much more than lower frequencies.

Keywords: Mesh-free method; Functionally graded piezoelectric beam; Free vibration; MLS shape function.

1 INTRODUCTION

IN recent years piezoelectric materials are considerably used in engineering applications as sensors and actuators. Deformation of piezoelectric materials causes generation of electric charge and conversely strain field is generated undergo applying an electric charge. This coupling property is widely considered to use in electrical and electro-mechanical devices. Traditional layered piezoelectric materials have some shortages such as cracking or creeping due to low or high temperature respectively and also abrupt change in the martial properties can cause stress concentration at interface. Concept of functionally graded materials (FGM) was introduced to overcome these shortages. Functionally graded piezoelectric materials are useful for many fields such as micro-electric- mechanical systems due to their continuously graded properties. Continuous variation of properties in special direction makes them suitable for reduction of stress concentration in piezoelectric materials which are used in sensors and actuators extensively. Static and dynamic analyses of FGPM structures can be used as an efficient tool in optimum design of

*Corresponding author.
E-mail address: foroutan@razi.ac.ir (M. Froutan).

sensors and actuators. Several works have been carried out using analytical methods to obtain dynamic and static response of FGPM structures. Sharma and Parashar [1] carried out free vibration analysis of shear induced FGPM annular plates by the generalized differential quadrature method. Kruusing [2] used an analytical method Based on the Euler-Bernoulli beam theory to obtain the mechanical response of an actuator with graded elastic constants. Hauke et al. [3] reported experimental results by using linear regression formula to determine deflection of FGPM actuator. Huang et al. [4] introduced analytical and semi-analytical solutions for anisotropic functionally graded magneto-electro-elastic beams subjected to an arbitrary load. Li and Feng [5] investigated free vibration analysis of FGPM beams using modified gradient method and Timoshenko beam theory. Wu and Syu [6] used perturbation method to obtain dynamic response of functionally graded piezoelectric cylindrical shells under electromechanical loads. Li and Peng [7] analyzed the static response of a FGPM spherical shell and an analytic method was considered to reduce problem to a Fredholm integral equation. Hsu [8] used deferential quadrature method (DQM) to investigate the electromechanical behavior of piezoelectric laminated composite beams. Razavi and Faramarzi Babadi [9] presented free vibration analysis FGPM cylindrical Nano shell based on consistent couple stress theory. They used energy method and Hamilton principle to determine the governing equations and boundary conditions. Zhang and Shi [10] focused on the response of a functionally graded piezoelectric (FGP) cylindrical actuator placed in a harmonic electric field based on elastic membrane theory and shell theory. They introduced non-dimensional expressions and an analytical solution for this type of actuators. Xiang and Shi [11] presented Static response of a multi-layered piezoelectric cantilever based on the Airy stress function.

Analytical methods are applicable for simple geometries with specific types of boundary conditions and external loads. Among numerical methods, the finite element method is a robust method for analysis of solid structures. In recent decades several work has been presented on static and dynamic analyses of FGPM structures by the finite element method. Transient response and vibration of FGPM beam under thermo-electro-mechanical load were studied by Doroushi and Eslami [12]. They used the higher order shear deformation and the finite element method to obtain the numerical results. Their results have been presented for various boundary conditions such as open and close circuit systems. Behjat and Khoshravan [13] investigated response of a FGP plate under mechanical and electrical loads by a nonlinear finite element analysis. Linearly inhomogeneous elements were used by Sedighi and Shakeri [14] for electrostatic analysis of simply supported FGP cylindrical panels. Behjat, et al. [15] presented static, free vibration and dynamic response of FGP panels by finite element method using four-node elements. Babaei and Chen [16] used finite element method to investigate thermo-piezoelectric response of FGP hollow cylinders under dynamic axisymmetric loading. FEM has some disadvantages such as difficulty of creating FEM meshes and low accuracy in stress calculation. Mesh-free methods are a new class of numerical methods, have been introduced recently as an alternative for the finite element method to simulate solid mechanics problems. In these methods a set of nodes are used for interpolation or approximation of unknown field variables. Mesh-free methods are classified into four categories based on the function approximation schemes; MLS approximation schemes, integral representation method, point interpolation methods and other mesh-free interpolation schemes [17]. Mesh-free methods have been improved by introducing MLS shape function, because continuous approximation is important features of MLS shape functions, which result in more accurate results. For the first time Nayroles et al. [18] used MLS shape function to promote the diffuse element method (DEM). Chuaqui and Roque [19] used multi quadric radial basis functions to investigate electro-mechanical static response of functionally graded piezoelectric smart subjected to mechanical loads and electric potential. MLS shape functions do not satisfy the Kronecker delta property. Therefore, in MLS based mesh- free methods, essential boundary conditions cannot be imposed directly as in the FEM. Among the methods have been used to impose essential boundary conditions in mesh-free methods, transformation method is more efficient than other methods. This method has been used in several works. Safaei and Moradi-Dastjerdi [20] analyzed natural frequencies of sandwich plates reinforced by functionally graded single-walled carbon nanotubes (SWCNTs) agglomerations by enforcing thermal loads. They used a mesh-free method based on MLS shape function to investigate the effects of essential boundary conditions. They applied the transformation method to impose essential boundary conditions. Moradi-Dastjerdi and Pourasghar [21] used the transformation method for imposition of essential boundary conditions in dynamic analysis of functionally graded nanocomposite cylinders reinforced by wavy carbon nanotube under an impact load. Moradi-Dastjerdi and Payganeh[22] studied thermoelastic dynamic behavior of functionally graded carbon nanotubes. They also applied the transformation method to modify a mesh-free method for imposition essential boundary conditions. Free vibration analysis of FGPM beams by a mesh-free method has not been carried out to the best of author's knowledge.

This work studies the free vibration analysis of FGPM beam by a mesh-free method based on weak form of two dimensional equations of motion and Maxwell's equation. MLS shape functions are used to approximate the displacement and electric potential fields in these equations. Since MLS approximation does not satisfy the

Kronecker delta, transformation method is applied to enforce the essential boundary conditions. The material properties vary smoothly across the thickness of the beam. After validation of the presented model, different slenderness ratio and various boundary conditions such as close and open circuits systems and clamped-free or clamped- clamped end conditions for beam are considered to present the results.

2 FORMULATION

2.1 Functionally graded piezoelectric material properties

The beam with FGPM properties, length L, and thickness h and negligible width b is made from mixture of two different materials with piezoelectric properties. According to 2-D, X-Y coordinate, it is assumed that properties vary smoothly through the thickness (Y direction) from top to bottom.

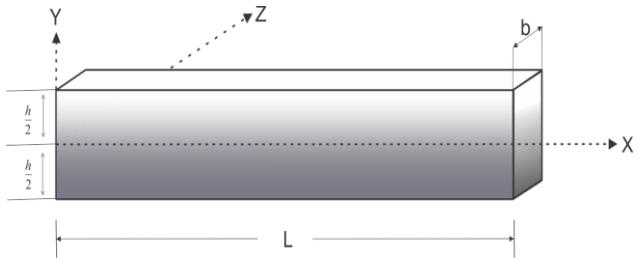

Fig.1
Geometry of rectangular FGPM beam.

According to law of mixture mechanical and electrical properties P of the functionally graded beam at each point are determined as follows:

$$P = P_{top}V_{top} + P_{bottom}V_{bottom} \tag{1}$$

where, P_{top} , V_{top} , P_{bottom} and V_{bottom} are property and volume fraction of material of top and bottom surfaces respectively. In this work, top and bottom surface materials are PZT-4 and PZT-5. Relation between V_{top} and V_{bottom} is explained as following:

$$V_{top} + V_{bottom} = 1 \tag{2}$$

A power law distribution proposed by Reddy and chin [23] is used for variation of volume fraction through the as follows:

$$V_{top} = \left(\frac{2y + h}{h}\right)^n \tag{3}$$

where n is the volume fraction index. Substituting Eqs. (3) and (2) in (1) leads to:

$$P(z) = \left(P_{top} - P_{bottom}\right)\left(0.5 + \frac{y}{h}\right)^n + P_{bottom} \tag{4}$$

2.2 Governing equations

The Hamilton's principle states that:

$$\delta\int_{t_1}^{t_2}(T - \Pi + W_{nc})dt = 0 \tag{5}$$

where, T, Π, and W_{nc} are kinetic energy, elastic strain energy, and the work done by external forces respectively. These variables are defined as follows:

$$T = \frac{1}{2}\int_{\Omega} \rho \dot{u}^T \dot{u} d\Omega \tag{6}$$

$$\Pi = \frac{1}{2}\int_{\Omega} \left(\varepsilon^T \sigma - E^T D\right) d\Omega \tag{7}$$

$$W_{nc} = \int_{\Omega} \left(u^T f_b - \Psi q_b\right) d\Omega + \int_{\Gamma} \left(u^T f_s - \Psi q_s\right) d\Gamma \tag{8}$$

where $\sigma, \varepsilon, E, \rho, D, u, \dot{u}, f_b, f_s, \Psi, q_b$ and q_s are stress vector, strain vector, electric field intensity, mass density, electric displacement, displacement vector, velocity vector, body force vector, surface traction vector, electrical potential, electrical body charge and electrical surface charge. Ω is the problem dominate and Γ is part of boundary on which surface tractions are enforced.

Also linear piezoelectric constitutive equations is demonstrated as follow [12]:

$$\sigma = C\varepsilon - e^T E \qquad D = e\varepsilon + \eta E \tag{9}$$

where, C, e, and η are stiffness, piezoelectric, and dielectric constant coefficient matrices, respectively. Substituting Eqs. (6), (7), (8) and (9) in (5) the weak form of governing equation is obtained:

$$\int \delta \left[\int_{\Omega} \frac{1}{2} \rho \dot{u}^T \dot{u} d\Omega - \int_{\Omega} \frac{1}{2} (\varepsilon^T C \varepsilon - \varepsilon^T e^T E - E^T e \varepsilon - E^T \eta E) d\Omega + \int_{\Omega} (u^T f_v - \Psi q_v) d\Omega + \int_{\Gamma} (u^T f_s - \Psi q_s) d\Gamma) \right] dt = 0 \tag{10}$$

In two dimensional coordinates $X-Y$, $\sigma, \varepsilon, C, e, \eta$ are expressed as:

$$\sigma = [\sigma_{xx} \quad \sigma_{yy} \quad \sigma_{xy}]^T \tag{11a}$$

$$\varepsilon = [\varepsilon_{xx} \quad \varepsilon_{yy} \quad \varepsilon_{xy}]^T \tag{11b}$$

$$C = \begin{bmatrix} C_{11} & C_{13} & 0 \\ C_{13} & C_{33} & 0 \\ 0 & 0 & C_{55} \end{bmatrix} \tag{11c}$$

$$e = \begin{bmatrix} 0 & e_{31} \\ 0 & e_{33} \\ e_{15} & 0 \end{bmatrix} \tag{11d}$$

$$\eta = \begin{bmatrix} \eta_{11} & 0 \\ 0 & \eta 33 \end{bmatrix} \tag{11e}$$

2.3 Mesh-free formulation

In MLS approximation, in domain Ω, variable $u(x)$ at interest point $X(x, y)$, is approximated by:

$$u(x) = \sum_{i=1}^{m} P_i(X) a_i = P^{\mathbf{T}}(X) a(X) \tag{12}$$

$P(X)$ is the basis function, $a(X)$ is coefficients which is function of x variable, and m is the number of monomials. In 2D problems linear basis function is given by:

$$P(X)=[1 \quad \mathrm{X} \quad \mathrm{Y}]^{\mathrm{T}} \tag{13}$$

$a(X)$ is determined by minimizing the following weighted residual:

$$J=\sum_{i=1}^{n} w(X-X_i)[P^{\mathrm{T}}(X)a(X)-\hat{u}_i]^2 \tag{14}$$

where n is the number of field nodes in the support domain Ω, $\hat{u}_i$ is the of virtual nodal value at node X_i, and w is the weight function. In this paper cubic spline is chosen as weight function

$$w(r_{ix})=\begin{cases} \frac{2}{3}-4r_{ix}^{\ 2}+4r_{ix}^{\ 3} & r_{ix}\le 0.5 \\ \frac{4}{3}-4r_{ix}+4r_{ix}^{\ 2}-\frac{4}{3}r_{ix}^{\ 3} & 0.5<r_{ix}\le 1 \\ 0 & 1<r_{ix} \end{cases} \tag{15}$$

$$r_{ix}=\frac{\|X-X_i\|}{d_{sx}}$$

$$w(r_{iy})=\begin{cases} \frac{2}{3}-4r_{iy}^{\ 2}+4r_{iy}^{\ 3} & r_{iy}\le 0.5 \\ \frac{4}{3}-4r_{iy}+4r_{iy}^{\ 2}-\frac{4}{3}r_{iy}^{\ 3} & 0.5<r_{iy}\le 1 \\ 0 & 1<r_{iy} \end{cases} \tag{16}$$

$$r_{iy}=\frac{\|Y-Y_i\|}{d_{sy}}$$

where, d_{cx} and d_{cy} are average node distances in X and Y directions, and α is the dimensionless size of the support domain.

$$d_{sx}=\alpha d_{cx} \qquad d_{sy}=\alpha d_{cy} \tag{17}$$

and

$$w(r)=w(r_{ix})\times w(r_{iy}) \tag{18}$$

Unknown coefficients $a(X)$ are determined by minimizing weighted residual:

$$\frac{\partial J}{\partial a}=0 \tag{19}$$

Consequently:

$$a(X)=[A(X)]^{-1}B(X)\,\hat{u} \tag{20}$$

In which

$$A(X)=\sum_{i=1}^{n} w(X-X_{\mathrm{i}})P(X_{\mathrm{i}})P^{\mathrm{T}}(X_{\mathrm{i}}) \tag{21}$$

and

$$B_{\mathbf{i}}=w(X-X_{\mathbf{i}})P(X_{\mathbf{i}}) \tag{22}$$

and $\hat{u}$ are virtual nodal values:

$$\hat{u}=[\hat{u}_1 \quad \hat{u}_2 \quad \dots \quad \hat{u}_n]^T \tag{23}$$

By replacing Eq. (20) to Eq. (12), Eq. (24) is obtained:

$$u(X)=\sum_{i=1}^{n}\Phi_i\hat{u}_i \tag{24}$$

where Φ_i is MLS shape function of node that located at $X=X_{\mathbf{i}}$:

$$\Phi_i(X)=P^{\mathbf{T}}(X)[A(X)]^{-1}B_{\mathbf{i}} \tag{25}$$

Displacement vector u and electrical potential ψ in X-Y coordinates can be approximated by the MLS shape functions:

$$u=\Phi_u\hat{u} \tag{26}$$

and

$$\Psi=\Phi_\psi\hat{\psi} \tag{27}$$

where

$$\Phi_u=\begin{bmatrix}\Phi_1 & 0 & \Phi_2 & 0 & \dots & \Phi_n & 0\\ 0 & \Phi_1 & 0 & \Phi_2 & \dots & 0 & \Phi_n\end{bmatrix} \tag{28}$$

$$\Phi_\psi=[\Phi_1 \quad \Phi_2 \quad \Phi_3 \quad \dots \quad \Phi_n] \tag{29}$$

where, the virtual displacement and virtual electric potential vectors are represented as:

$$\begin{aligned}&\hat{\psi}=[\hat{\psi}^1 \quad \hat{\psi}^2 \quad \hat{\psi}^3 \quad \dots \quad \hat{\psi}^n]^T\\ &\boldsymbol{u}=\left[u_1\ u_2\ \dots..\ u_n\right]^T\end{aligned} \tag{30}$$

The equations for strain and electrical field are provided which related theme to displacement and electrical potential respectively:

$$\varepsilon=B_u\hat{u} \tag{31}$$

$$E=-B_\psi\hat{\psi} \tag{32}$$

In which B_u and B_ψ , are given as:

$$B_u = \begin{bmatrix} \frac{\partial \Phi_1}{\partial x} & 0 & \dots & \frac{\partial \Phi_n}{\partial x} & 0 \\ 0 & \frac{\partial \Phi_1}{\partial y} & \dots & 0 & \frac{\partial \Phi_n}{\partial y} \\ \frac{\partial \Phi_1}{\partial y} & \frac{\partial \Phi_1}{\partial x} & \dots & \frac{\partial \Phi_n}{\partial y} & \frac{\partial \Phi_n}{\partial x} \end{bmatrix} \tag{33}$$

$$B_\psi = \begin{bmatrix} \frac{\partial \Phi_1}{\partial x} & \frac{\partial \Phi_2}{\partial x} & \dots & \frac{\partial \Phi_n}{\partial x} \\ \frac{\partial \Phi_1}{\partial y} & \frac{\partial \Phi_2}{\partial y} & \dots & \frac{\partial \Phi_n}{\partial y} \end{bmatrix} \tag{34}$$

By replacing Eq. (26), (27), (31) and (32) in Eq. (10) and by neglecting body forces and electrical body charge, mesh-free formulation is demonstrated as:

$$\begin{aligned} &\delta(\hat{u}\ )^T \left(\int_\Lambda B_u^T C B_u d\Omega \right) \hat{u}\ + \delta(\hat{u}\ )^T \left(\int_\Lambda \rho \Phi_u^T \Phi_u d\Omega \right) \ddot{\hat{u}} + \delta(\hat{u})^T \left(\int_\Lambda B_u^T e B_\psi d\Omega \right) \hat{\psi} - \delta(\hat{u}\ )^T \int_{s_f} \Phi_u^T f_s d\Gamma = 0 \\ &\delta(\hat{\psi})^T \left(\int_\Lambda B_\psi^T e B_u d\Omega \right) \hat{u}\ - \delta(\hat{\psi})^T \left(\int_\Lambda B_\psi^T \eta B_\psi d\Omega \right) \hat{\psi} - \delta(\hat{\psi})^T \int_{s_f} \Phi_\psi^T q_s d\Gamma = 0 \end{aligned} \tag{35}$$

By rearranging Eq. (35) with coefficients of $\delta(\hat{u})$ and $\delta(\hat{\psi})$ leads to:

$$\begin{aligned} &\left(\int_\Lambda B_u^T C B_u d\Omega \right) \hat{u}\ + \left(\int_\Lambda \rho \Phi_u^T \Phi_u d\Omega \right) \ddot{\hat{u}} + \left(\int_\Lambda B_u^T e B_\psi d\Omega \right) \hat{\psi} - \int_{s_f} \Phi_u^T f_s d\Gamma = 0 \\ &\left(\int_\Lambda B_\psi^T e B_u d\Omega \right) \hat{u}\ - \left(\int_\Lambda B_\psi^T \eta B_\psi d\Omega \right) \hat{\psi} - \int_{s_f} \Phi_\psi^T q_s d\Gamma = 0 \end{aligned} \tag{36}$$

or:

$$\hat{M}\, \overset{\circ\circ}{\hat{U}} + \hat{K}_{uu} \hat{U} + \hat{K}_{u\psi} \hat{\psi} = \hat{f}_u \qquad\qquad \hat{K}_{\psi\circ} \hat{U} + \hat{K}_{\psi\psi} \hat{\psi} = \hat{f}_\psi \tag{37}$$

where:

$$\hat{U} = [\hat{u}_x^1 \quad \hat{u}_y^1 \quad \dots \quad \hat{u}_x^N \quad \hat{u}_y^N]^T \qquad\qquad \hat{\Psi} = [\hat{\psi}^1 \quad \hat{\psi}^2 \quad \hat{\psi}^3 \quad \dots \quad \hat{\psi}^N]^T \tag{38}$$

and

$$\begin{aligned} &\hat{M} = \int_\Lambda \rho \Phi_u^T \Phi_u d\Omega \\ &\hat{K}_{uu} = \int_\Lambda \mathrm{B}_u^T \mathrm{C} \mathrm{B}_u d\Omega \qquad \hat{K}_{u\psi} = \int_\Lambda \mathrm{B}_u^T \mathrm{e} \mathrm{B}_\psi d\Omega \qquad \hat{K}_{\psi u} = \int_\Lambda \mathrm{B}_\psi^T \mathrm{e} \mathrm{B}_u d\Omega \qquad \hat{K}_{\psi\psi} = -\int_\Lambda \mathrm{B}_\psi^T \eta \mathrm{B}_\psi d\Omega \\ &\hat{f}_u = \int_{s_f} \Phi_u^T f_s d\Gamma \qquad \hat{f}_\psi = \int_{s_f} \Phi_\psi^T q_s d\Gamma \end{aligned} \tag{39}$$

For free vibration $\hat{f}_u$ and $\hat{f}_\psi$ are zero. These matrices can be calculated easily by numerical integration. To impose essential boundary conditions, displacement and electrical potential nodal value vector must have the real values. Because $\hat{U}$ and $\hat{\Psi}$ have virtual value, essential boundary conditions cannot be imposed directly. Transformation is a simple method which is established for mesh-free to turn virtual displacement $\left(\hat{U}\right)$ and electrical potential $\left(\hat{\Psi}\right)$ into the real values. In this method, real and virtual nodal values are related by transformation matrices:

$$U = T_u \hat{U} \qquad \Psi = T_\psi \hat{\Psi} \tag{40}$$

where

$$\begin{aligned} U &= \begin{bmatrix} u_x^1 & u_y^1 & \dots & u_x^N & u_y^N \end{bmatrix}^T \\ \Psi &= [\psi^1 \quad \psi^2 \quad \psi^3 \quad \dots \quad \psi^N]^T \end{aligned} \tag{41}$$

$$T_u = \begin{bmatrix} \Phi_1(X_1) & 0 & \Phi_2(X_1) & 0 & \dots & \Phi_N(X_1) & 0 \\ 0 & \Phi_1(X_1) & 0 & \Phi_2(X_1) & \dots & 0 & \Phi_N(X_1) \\ \vdots & \vdots & \vdots & \vdots & \vdots & \vdots & \vdots \\ \Phi_1(X_N) & 0 & \Phi_2(X_N) & 0 & \dots & \Phi_N(X_N) & 0 \\ 0 & \Phi_1(X_N) & 0 & \Phi_2(X_N) & \dots & 0 & \Phi_N(X_N) \end{bmatrix} \tag{42}$$

$$T_\psi = \begin{bmatrix} \Phi_1(X_1) & \Phi_2(X_1) & \dots & \Phi_N(X_1) \\ \Phi_1(X_2) & \Phi_2(X_2) & \dots & \Phi_N(X_2) \\ \vdots & \vdots & \vdots & \vdots \\ \Phi_1(X_N) & \Phi_2(X_N) & \dots & \Phi_N(X_N) \end{bmatrix}$$

Eq. (43) for free vibration is obtained by rearranging Eq. (37):

$$\begin{aligned} M\ddot{U} + K_{uu}U + K_{u\psi}\Psi &= 0 \\ K_{\psi u}U + K_{\psi\psi}\Psi &= 0 \end{aligned} \tag{43}$$

$$\begin{aligned} M &= (T_u^{-1})^T \hat{M} T_u^{-1} \\ K_{uu} &= (T_u^{-1})^T \hat{K}_{uu} T_u^{-1} \\ K_{u\psi} &= (T_u^{-1})^T \hat{K}_{u\psi} T_\psi^{-1} \\ K_{\psi u} &= (T_\psi^{-1})^T \hat{K}_{\psi u} T_u^{-1} \\ K_{\psi\psi} &= (T_\psi^{-1})^T \hat{K}_{\psi\psi} T_\psi^{-1} \end{aligned} \tag{44}$$

Essential boundary conditions can be implemented directly to Eq. (43). By solving Eq. (43):

$$\Psi = -K_{\psi\psi}^{-1} * K_{\psi u} U \tag{45}$$

Replacing Eq. (45), in Eq. (43) leads to:

$$M\ddot{U} + K_{eq}U = 0 \tag{46}$$

where:

$$K_{eq} = K_{uu} - K_{u\psi} K_{\psi\psi}^{-1} K_{\psi u} \tag{47}$$

3 NUMERICAL RESULTS AND DISCUAAION

First of all, the convergence of the method is important to obtain reliable number of nodes to present the results. The first three dimensionless natural frequencies $\Omega = \omega h \sqrt{(\rho / c_{11})_{PZT-4}}$ with clamped-free as mechanical boundary condition, are shown in Table 1., for different node arrangements.

Table 1
Convergency study of the meshless method, first three natural frequencies of a Clamped-Free FGPM beam (*L/h*=5, *n*=0.1).

Nodes distribution	2*6	3*11	5*21	6*26	7*31	8*36
Ω_1	0.0341	0.0271	0.0363	0.0377	0.0374	0.0374
Ω_2	0.1886	0.2078	0.2038	0.2038	0.2035	0.2034
Ω_3	0.2925	0.2988	0.2983	0.2982	0.2981	0.2981

Because of small difference between results obtained with 6*26 and 7*31 node arrangements, 6*26 nodes have been selected to report the results with reliable accuracy.

Table 2
Materials constants [12].

Material	c_{11}	c_{13}	c_{33}	c_{55}	e_{13}	e_{33}	e_{15}	η_{11}	η_{33}
PZT-4	139	74.3	115	25.6	-5.2	15.1	12.7	1.306	1.151
PZT-5H	127.2	84.67	117.44	22.99	-6.62	23.24	17.03	2.771	3.010

In this study FGPM properties have been considered to present the results. In FGPM beam, properties are varied form bottom surface which is PZT-5H to PZT-4 at the top. The material properties of FGPM are listed in Table 2.

Table 3
The first three dimensionless natural frequencies of a FGPM beam (*n*=0).

	Ref	Pre	Diff%	Ref	Pre	Diff%
C-F		*L/h=5*			*L/h=15*	
Ω_1	0.0392	0.0381	2.8	0.0045	0.0044	2.2
Ω_2	0.2080	0.2060	0.0	0.0275	0.0268	2.5
Ω_3	0.3306	0.3017	8.7	0.0744	0.0714	4.0
C-C						
Ω_1	0.2025	0.2050	1.2	0.0277	0.0273	1.0
Ω_2	0.4608	0.4803	4.2	0.0733	0.0713	2.7
Ω_3	0.6575	0.6043	8.0	0.1369	0.1343	1.8

Table 4
The first three dimensionless natural frequencies of a clamped-free FGPM beam (*L/h*=15).

	n=0	*n*=0.2	*n*=1	*n*=10
Ω_1	0.0044	0.0040	0.0040	0.0040
Ω_2	0.0268	0.0256	0.0250	0.0235
Ω_3	0.0714	0.0696	0.0663	0.0641

The first three natural frequencies, obtained from the presented model are compared with those presented by Doroushi et al. [12] in Table 3. Diff is defined as $Diff\ \% = \frac{\Omega_r - \Omega_p}{\Omega_r} * 100$ that show difference between reference results and present study. Ω_r and Ω_p are the results reported by reference and present study, respectively. Accuracy of

results obtained from beam theories increases with increase in slenderness ratio. This factor does not affect the accuracy of results obtained from 2-dimensional theory of elasticity. That is why the difference between results are significant for lower values of *L*/*h* ratio. Furthermore, this table shows that natural frequencies with C-C boundary condition are greater than those with C-F boundary condition as expected. Effect of power exponent *n* on natural frequencies is shown in Table 4. This table depicts that natural frequencies decrease with increase of *n*. Increase in power index *n* leads to increase in volume fraction of PZT-5H and consequently decrease in stiffness of the beam. This can justify the decrease in natural frequencies with increase of *n*.

Table 5
The first three dimensionless natural frequencies of a clamped-free FGPM beam (*n*=1).

	L/h=5	*L/h=10*	*L/h=12*	*L/h=15*
Ω_1	0.0365	0.0089	0.0061	0.0040
Ω_2	0.1963	0.0551	0.0373	0.0250
Ω_3	0.2831	0.1417	0.1004	0.0663

Table 5., shows the effect of ratio *L*/*h* on natural frequencies. Natural frequencies decrease with increase in this ratio because of decrease in stiffness of the beam. In order to study the effect of *n* and *L*/*h* on natural frequencies, variation of first three frequencies versus *L*/*h* for different values on *n* are shown in Fig. 2. This figure confirms the results obtained from Tables 4 and 5. Furthermore this figure reveals that the *L*/*h* ratio has more significant effect on lower frequencies. On the other hand higher frequencies are affected by n much more than lower frequencies.

Table 6
The first three dimensionless natural frequencies in open and close circuits of a Clamped-Free FGPM beam (*L/h*=10).

	open *n*=0	close *n*=0	Diff%	open *n*=1	close *n*=1	Diff%	open *n*=10	close *n*=10	Diff%
Ω_1	0.0095	0.0095	0.0	0.0089	0.0089	0.0	0.0085	0.0083	2.3
Ω_2	0.0567	0.0560	1.2	0.0551	0.0537	2.5	0.0507	0.0501	1.1
Ω_3	0.1526	0.1453	4.7	0.1417	0.1360	4.0	0.1336	0.1276	4.5

To examine effect of electrical boundary conditions on natural frequencies, results are obtained for open loop and closed loop conditions and summarized in Table 6. For closed loop condition, mechanical energy of the system is converted to electrical energy and consequently the stiffness of system decreases. That is why natural frequencies for closed loop condition are less than those for open loop condition.

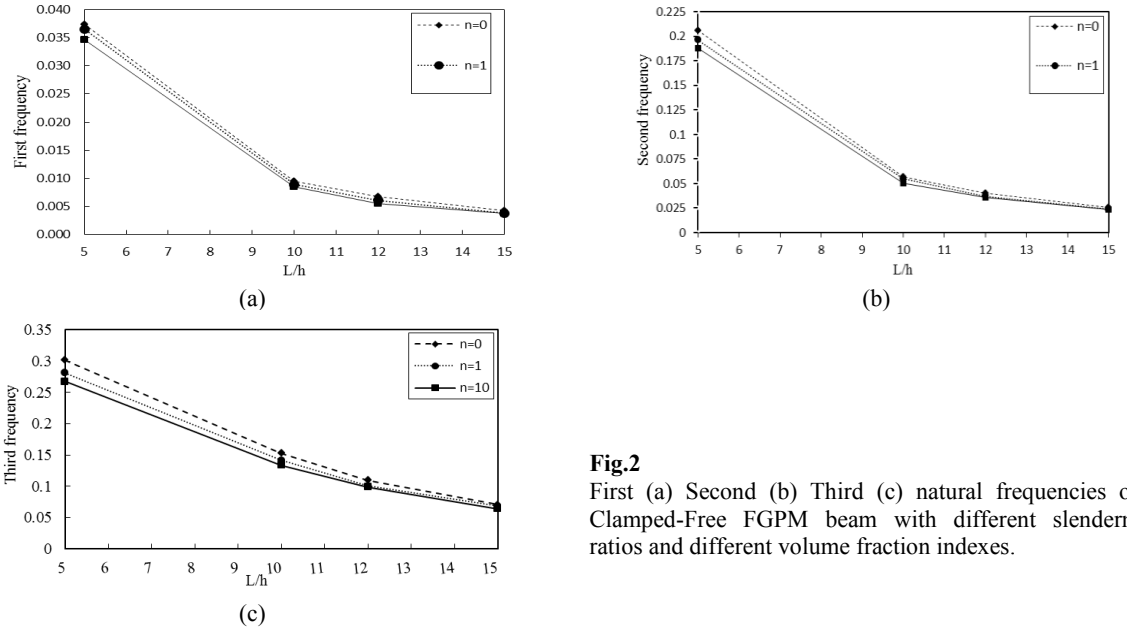

Fig.2
First (a) Second (b) Third (c) natural frequencies of a Clamped-Free FGPM beam with different slenderness ratios and different volume fraction indexes.

4 CONCLUSIONS

Free vibration of functionally graded piezoelectric beams subjected to different boundary conditions was investigated using a mesh-free method. The formulation is based on 2-D elasticity theory and governing equations are derived by Hamilton principle. PZT-4 and PZT-5H are used as constituent materials in this study. Effect of ratio *L/h*, power exponent n and electrical boundary conditions on natural frequencies of beam were investigated by the presented model. It was concluded that the ratio *L/h* has more effect on lower frequencies while, effect of power exponent n on higher frequencies is more significant. Natural frequencies with open loop condition are greater than those with closed loop condition.

REFERENCES

[1] Sharma P., Parashar S.K., 2016, Free vibration analysis of shear-induced flexural vibration of FGPM annular plate using Generalized Differential Quadrature method, *Composite Structures* **155**: 213-222.

[2] Kruusing A., 2000, Analysis and optimization of loaded cantilever beam microactuators, *Smart Materials and Structures* **9**(2): 186.

[3] Hauke T., 2000, Bending behavior of functionally gradient materials, *Ferroelectrics* **238**(1): 195-202.

[4] Huang D., Ding H., Chen W., 2010, Static analysis of anisotropic functionally graded magneto-electro-elastic beams subjected to arbitrary loading, *European Journal of Mechanics-A/Solids* **29**(3): 356-369.

[5] Li Y., Feng W., Cai Z., 2014, Bending and free vibration of functionally graded piezoelectric beam based on modified strain gradient theory, *Composite Structures* **115**: 41-50.

[6] Wu C.-P., Syu Y.-S., 2007, Exact solutions of functionally graded piezoelectric shells under cylindrical bending, *International Journal of Solids and Structures* **44**(20): 6450-6472.

[7] Li X.-F., Peng X.-L., Lee K.Y., 2010, The static response of functionally graded radially polarized piezoelectric spherical shells as sensors and actuators, *Smart Materials and Structures* **19**(3): 035010.

[8] Hsu M.-H., 2005, Electromechanical analysis of piezoelectric laminated composite beams, *Journal of Marine Science and Technology* **13**(2): 148-155.

[9] Razavi H., Babadi A.F., Beni Y.T., 2017, Free vibration analysis of functionally graded piezoelectric cylindrical nanoshell based on consistent couple stress theory, *Composite Structures* **160**: 1299-1309.

[10] Zhang T., Shi Z., Spencer Jr B., 2008, Vibration analysis of a functionally graded piezoelectric cylindrical actuator, *Smart Materials and Structures* **17**(2): 025018.

[11] Xiang H., Shi Z., 2009, Static analysis for functionally graded piezoelectric actuators or sensors under a combined electro-thermal load, *European Journal of Mechanics-A/Solids* **28**(2): 338-346.

[12] Doroushi A., Eslami M., Komeili A., 2011, Vibration analysis and transient response of an FGPM beam under thermo-electro-mechanical loads using higher-order shear deformation theory, *Journal of Intelligent Material Systems and Structures* **22**(3): 231-243.

[13] Behjat B., Khoshravan M., 2012, Geometrically nonlinear static and free vibration analysis of functionally graded piezoelectric plates, *Composite Structures* **94**(3): 874-882.

[14] Sedighi M., Shakeri M., 2009, A three-dimensional elasticity solution of functionally graded piezoelectric cylindrical panels, *Smart Materials and Structures* **18**(5): 055015.

[15] Behjat B., 2009, Static, dynamic, and free vibration analysis of functionally graded piezoelectric panels using finite element method, *Journal of Intelligent Material Systems and Structures* **20**(13): 1635-1646.

[16] Babaei M., Chen Z., 2009, The transient coupled thermo-piezoelectric response of a functionally graded piezoelectric hollow cylinder to dynamic loadings, *Proceedings of the Royal Society of London A: Mathematical, Physical and Engineering Sciences*.

[17] Liu G., Gu Y., 2005, *An Introduction to Meshfree Methods and Their Programming,* Springer, Dordrecht, Netherlands.

[18] Nayroles B., Touzot G., Villon P., 1992, Generalizing the finite element method: diffuse approximation and diffuse elements, *Computational Mechanics* **10**(5): 307-318.

[19] Chuaqui T., Roque C., 2017, Analysis of functionally graded piezoelectric timoshenko smart beams using a multiquadric radial basis function method, *Composite Structures* **176**: 640-653.

[20] Safaei B., Moradi-Dastjerdi R., Chu F., 2018, Effect of thermal gradient load on thermo-elastic vibrational behavior of sandwich plates reinforced by carbon nanotube agglomerations, *Composite Structures* **192**: 28-37.

[21] Moradi-Dastjerdi R., Pourasghar A., 20216, Dynamic analysis of functionally graded nanocomposite cylinders reinforced by wavy carbon nanotube under an impact load, *Journal of Vibration and Control* **22**(4): 1075-1062.

[22] Moradi-Dastjerdi R., Payganeh G., 2017, Thermoelastic dynamic analysis of wavy carbon nanotube reinforced cylinders under thermal loads, *Steel and Composite Structures* **25**(3): 315-326.

[23] Reddy J., Chin C., 1998, Thermomechanical analysis of functionally graded cylinders and plates, *Journal of Thermal Stresses* **21**(6): 593-626.